

## Article

# 3-Aryl-5-aminobiphenyl Substituted [1,2,4]triazolo[4,3-*c*]quinazolines: Synthesis and Photophysical Properties

Alexandra E. Kopotilova <sup>1</sup>, Tatyana N. Moshkina <sup>1</sup>, Emiliya V. Nosova <sup>1,2,\*</sup> , Galina N. Lipunova <sup>2</sup>, Ekaterina S. Starnovskaya <sup>1,2</sup>, Dmitry S. Kopchuk <sup>1,2</sup>, Grigory A. Kim <sup>1,2</sup> , Vasiliy S. Gaviko <sup>1,3</sup>, Pavel A. Slepukhin <sup>1,2</sup> and Valery N. Charushin <sup>1,2</sup> 

<sup>1</sup> Department of Organic and Biomolecular Chemistry, Ural Federal University, 620002 Ekaterinburg, Russia

<sup>2</sup> I. Postovsky Institute of Organic Synthesis, Ural Branch of the Russian Academy of Sciences, 620108 Ekaterinburg, Russia

<sup>3</sup> M.N. Mikheev Institute of Metal Physics, Ural Branch of the Russian Academy of Sciences, 620108 Ekaterinburg, Russia

\* Correspondence: emilia.nosova@yandex.ru

**Abstract:** Amino-[1,1′]-biphenyl-containing 3-aryl-[1,2,4]triazolo[4,3-*c*]quinazoline derivatives with fluorescent properties have been designed and synthesized. The type of annelation of the triazole ring to the pyrimidine one has been unambiguously confirmed by means of an X-ray diffraction (XRD) method; the molecules are non-planar, and the aryl substituents form the pincer-like conformation. The UV/Vis and photoluminescent properties of target compounds were investigated in two solvents of different polarities and in a solid state. The samples emit a broad range of wavelengths and display fluorescent quantum yields of up to 94% in toluene solutions. 5-(4′-Diphenylamino-[1,1′]-biphenyl-4-yl)-3-(4-(trifluoromethyl)phenyl)-[1,2,4]triazolo[4,3-*c*]quinazoline exhibits the strongest emission in toluene and a solid state. Additionally, the solvatochromic properties were studied for the substituted [1,2,4]triazolo[4,3-*c*]quinazolines. Moreover, the changes in absorption and emission spectra have been demonstrated upon the addition of water to MeCN solutions, which confirms aggregate formation, and some samples were found to exhibit aggregation-induced emission enhancement. Further, the ability of triazoloquinazolines to detect trifluoroacetic acid has been analyzed; the presence of TFA induces changes in both absorption and emission spectra, and acidochromic behavior was observed for some triazoloquinazoline compounds. Finally, electronic-structure calculations with the use of quantum-chemistry methods were performed for synthesized compounds.

**Keywords:** [1,2,4]triazolo[4,3-*c*]quinazolines; cross-coupling; fluorescence; solvatochromism; pH-sensor



**Citation:** Kopotilova, A.E.; Moshkina, T.N.; Nosova, E.V.; Lipunova, G.N.; Starnovskaya, E.S.; Kopchuk, D.S.; Kim, G.A.; Gaviko, V.S.; Slepukhin, P.A.; Charushin, V.N. 3-Aryl-5-aminobiphenyl Substituted [1,2,4]triazolo[4,3-*c*]quinazolines: Synthesis and Photophysical Properties. *Molecules* **2023**, *28*, 1937. <https://doi.org/10.3390/molecules28041937>

Academic Editors: Athanassios C. Tsipis and Alexey M. Starosotnikov

Received: 24 January 2023

Revised: 9 February 2023

Accepted: 13 February 2023

Published: 17 February 2023



**Copyright:** © 2023 by the authors. Licensee MDPI, Basel, Switzerland. This article is an open access article distributed under the terms and conditions of the Creative Commons Attribution (CC BY) license (<https://creativecommons.org/licenses/by/4.0/>).

## 1. Introduction

Heterocyclic scaffolds containing the triazole rings, which are annelated with natural pyrimidine heterocycles, represent “lead compounds” for organic synthesis [1], medicinal chemistry [2] and pharmacology [3,4]. Recently, the ability of some [1,2,4]triazolo[4,3-*c*]quinazolines to act as penetrating DNA intercalators has been demonstrated [5,6]. 3,5-Diphenyl[1,2,4]triazolo[4,3-*c*]quinazoline was reported as a selective A<sub>3</sub>A adenosine receptor antagonist [7], and 5-aryl-[1,2,4]triazolo[4,3-*c*]quinazoline-3-amine demonstrated anticonvulsant activity [8].

The main advantage of the azolodiazine domain of 1,2,4-triazole-containing hybrid molecules is associated with a planarized skeleton of aza-heterocyclic core, which has an important effect on structural modifications [9], biological interactions [10] and chromophore properties [11]. Benzoimidazo[1,2-*a*][1,2,3]triazolo[4,5-*e*]pyrimidines **A** (Figure 1) demonstrated aggregation-induced emissions (AIE) and acidochromic behaviour [12]. The emission spectra of 2*H*-[1,2,3]triazolo[4,5-*e*][1,2,4]triazolo[1,5-*a*]pyrimidine derivatives **B** in

acetonitrile solutions are sensitive to the presence of nitroaromatic explosives [13]. Fluorescent 2-aryl-1,2,3-triazolopyrimidine **C** was demonstrated to penetrate cells and selectively accumulate in the cell membrane, Golgi complex and endoplasmic reticulum, which opens up wide opportunities in bioimaging [11].

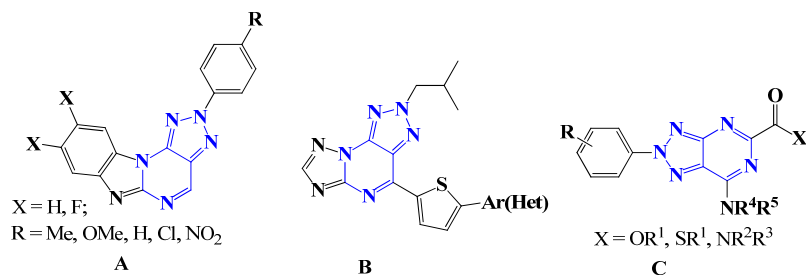


**Figure 1.** Representatives of triazolopyrimidine-containing chromophores (A–C).

The quinazolinyl moiety possesses a stronger electron-withdrawing ability than the pyrimidinyl core due to extra electron delocalization into the fused benzene ring. Enhanced intramolecular charge transfer (ICT) in quinazoline chromophores was illustrated by red-shifted absorption and emission with regard to their pyrimidine analogs [14]. There is limited data on the optical properties of 3,5-diarylsubstituted [1,2,4]triazolo[4,3-*c*]quinazolines. 5-Fluorenyl-, 5-spirofluorenyl and 5-(3(4)-fluorenyl)phenyl substituted 3-(4-cyanophenyl)-[1,2,4]triazolo[4,3-*c*]quinazolines (compounds **D–F**, Figure 2) were reported as novel electron transport heterocycles for efficient OLED materials possessing proper molecular dipole moments, which are able to be in compact contact with other organic layers in the process of forming a device [15]. Analogs of compounds **D–F** bearing a triphenyl-1,3,5-triazine fragment instead of a cyanophenyl one were mentioned in patent [16], and some 5-phenyl-, 5-biphenyl- and 5-naphthyl- derivatives of [1,2,4]triazolo[4,3-*c*]quinazolines containing triphenyl-1,3,5-triazine residue in position C(3) have been developed [17].

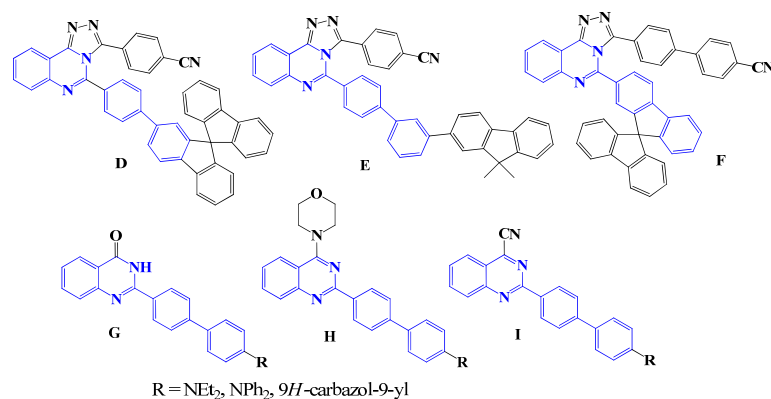


**Figure 2.** Representatives of biphenyl-substituted quinazoline chromophores **D–I**.

Our research group is working on synthetic approaches to quinazoline fluorophores and investigating the photophysical properties, as well as possible practical applications. Recently, the  $\pi$ -conjugated chromophores based on 2-aryl/thienyl-4-cyanoquinazolines, including 2-(4'-amino[1,1'-biphenyl]-4-yl)-containing derivatives **G–I** (Figure 2), have been studied [18,19]. 4-Cyanoquinazolines are shown to be less emissive in solvents and solid state than quinazolin-4-ones [19] and morpholinyl [20] counterparts; the introduction of the cyano group into position C(4) leads to orange/red coloured powder and dual emission bands [19]. Annellation of the triazole cycle can be considered another way to enhance the electron-acceptor character of the quinazoline core.

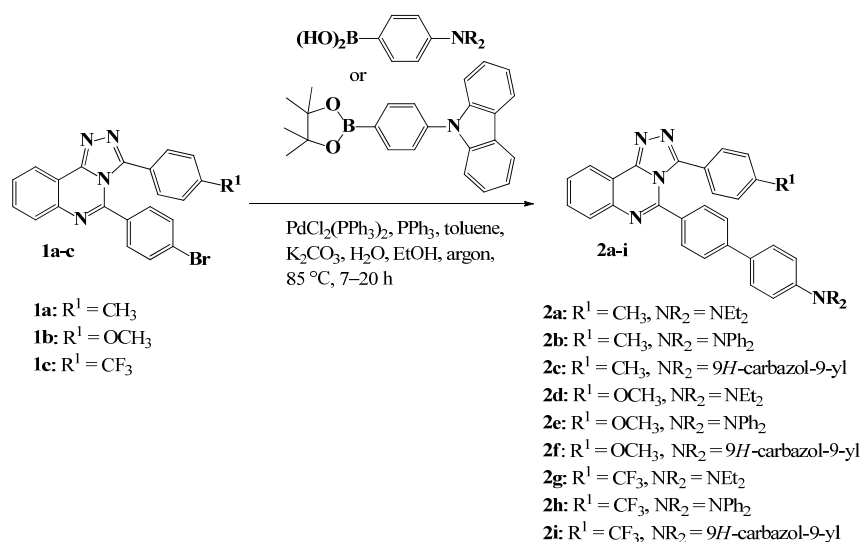
Herein, we develop the series of [1,2,4]triazolo[4,3-*c*]quinazolines bearing 3-aryl and 5-aminobiphenyl fragments to handle the detailed investigation of photophysical properties

and to discover preferable structures for practical applications. The synthetic approach involves the cross-coupling of a bromo-derivative with boronic acid under typical conditions. The target compounds appeared to exhibit fluorescent properties both in solution and solid state; the fluorophores demonstrated changes in absorption and emission spectra upon the addition of water to MeCN solutions. Moreover, triazoloquinazolines show sensing properties toward acid.

## 2. Results

### 2.1. Synthesis

Triazoloquinazoline fluorophores **2a–i** were obtained by a Suzuki–Miyaura cross-coupling reaction. The approach involves a Pd-catalyzed interaction of the corresponding 4-bromophenyl derivative **1a–c** with arylboronic acid or an arylboronic acid pinacol ester; the yields were from moderate to good (25–65%), Scheme 1. The starting 3-(*p*-tolyl), 3-(4-methoxyphenyl) or 3-(4-trifluoromethyl) substituted 5-(4-bromophenyl)-[1,2,4]triazolo[4,3-*c*]quinazolines **1a–c** were prepared from appropriate hydrazones by oxidative cyclization with bromine in glacial acetic acid at room temperature, as previously described [21].



**Scheme 1.** Synthesis of 3-aryl-5-(4'-amino[1,1']-biphenyl)[1,2,4]triazolo[4,3-*c*]quinazolines **2a–i**.

$^1\text{H}$  NMR,  $^{13}\text{C}$  NMR spectroscopy, mass spectrometry (Supplementary Materials—Figures S1–S9) and elemental analysis data confirmed the identity and purity of target compounds.  $^{13}\text{C}$  NMR data for sample **2i** has not been obtained due to its poor solubility in organic solvents, including DMSO- $d_6$  under heating.

Single crystals of quinazolines **2a** and **2e** were obtained by a slow evaporation technique (MeCN and *n*-hexane/chloroform mixture, respectively, used as a solvent) and analyzed by an X-ray diffraction method (XRD) (Figure 3, Supplementary Materials—Tables S1–S4, Figure S10). According to XRD data, compound **2a** is crystallized in the centrosymmetric space group of the monoclinic system. The molecule is non-planar, and the aryl substituents form the pincer-like conformation (Figure 3). The mean bond lengths and angles are near expectations. The configuration of the nitrogen atom in the diethyl amino group is near to planar. The deviation of the N(34) atom from the plane C(31)C(35)C(37) is 0.099 Å. The C–N bond distances of the ethyl substituents at the amino moiety are varied within a range of 1.456–1.462 Å. The distance C(31)–N(34) of 1.387 Å is significantly shortened, and the conjugation between the N(34) atom and the aryl substituent is observed. The shortened  $\pi$ - $\pi$  interactions between the heterocyclic part and  $\pi$ -donating  $\text{NEt}_2$ -phenyl substituent are observed, the distance C(5) . . . C(29) [ $1 - x, y - 0.5, 1.5 - z$ ] was found to be 3.274 Å, which is 0.13 Å less than sum of the V-d-W radii.

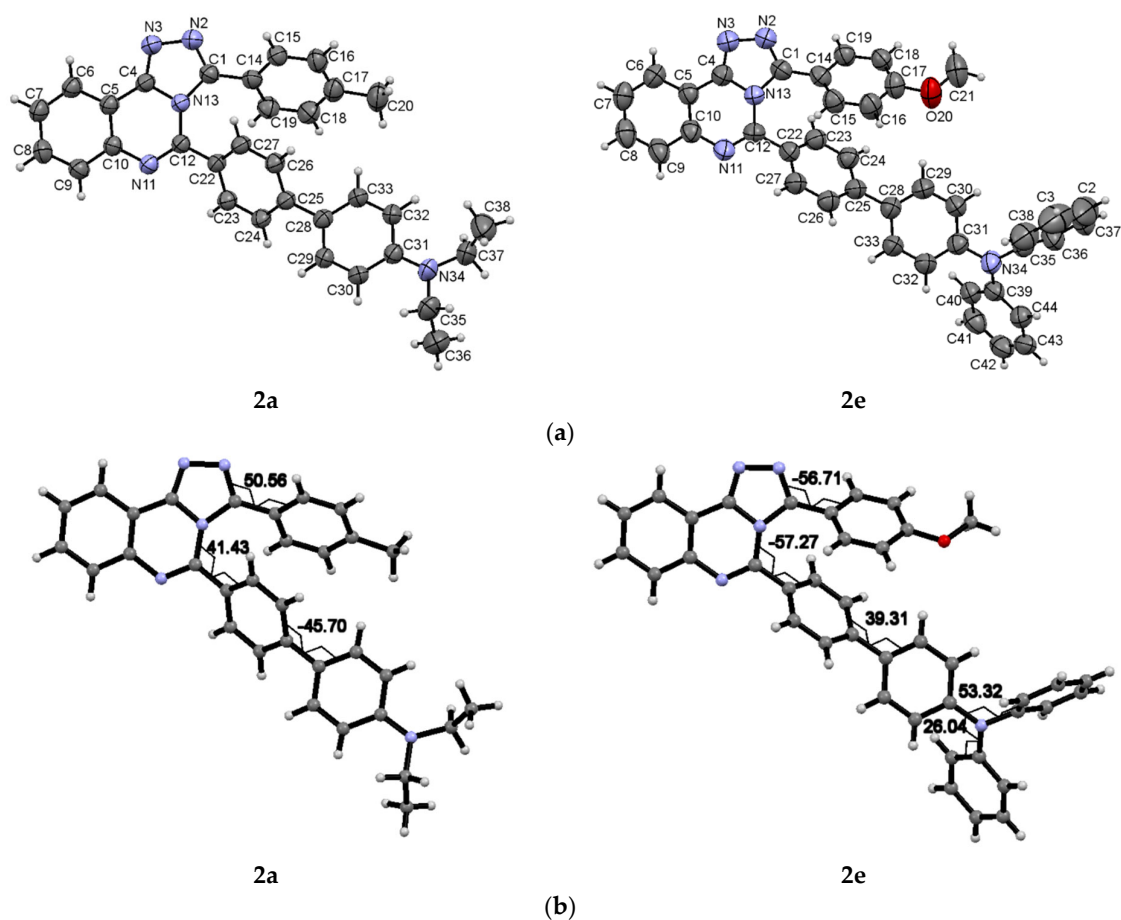


**Figure 3.** (a) Molecular structure of **2a** and **2e** in the thermal ellipsoids of 50% probability. (b) Selected torsion angles of compounds **2a** and **2e**.

Compound **2e** is crystallized in the non-primitive centrosymmetric space group. As well as **2a**, molecule **2e** is non-planar, and the aryl substituents form the pincer-like conformation (Figure 3). The mean bond lengths and angles were also close to expectations. The three N–C bonds at the triaryl amino group are almost in the same plane. The deviation of the N(34) atom from the C(31)C(35)C(39) plane is 0.10 Å, significant torsion angles were defined between all aryl substituents and the plane of the C–N bonds. The C–N bond distances of the triaryl amino moiety are varied within the range of 1.409–1.443 Å. The T-shaped  $Csp^2-H \cdots N$   $\pi$ -contacts take place with the participation of the nitrogen atom of the triazolo moiety. No shortened  $\pi$ - $\pi$  interactions in the molecular packing were found.

An undoubted significance of the XRD data obtained for compounds **2a**, **e** is that the type of annelation of the triazole moiety to the quinazoline one has been unambiguously confirmed. Unfortunately, there is still conflicting information in the literature; in particular, some patents report the formation of the [4,3-*c*] isomer of triazoloquinazoline [15,17] from arylhydrazone, and others state the [1,5-*c*] isomer [16] in the presence of the same oxidant  $PhI(OAc)_2$ . Evidence of structure, causes of different reactions, and Dimroth rearrangement conditions were not provided.

## 2.2. UV/Vis and Fluorescence Spectroscopy

The UV/Vis absorption and photoluminescence (PL) spectroscopic data for toluene and MeCN solutions of [1,2,4]triazolo[4,3-*c*]quinazoline fluorophores **2a–i** are presented in Table 1; the corresponding spectra are shown in Supplementary Materials Figures S11–S23. The solutions of a  $c \approx 10^{-5}$  M concentration were prepared for the experiments.

**Table 1.** Photophysical properties of [1,2,4]triazolo[4,3-*c*]quinazolines **2a–i** in toluene and MeCN solutions.

Compound	Solvent	$\lambda_{\text{abs}}$ , nm ( $\epsilon$ M, $10^4$ M <sup>-1</sup> cm <sup>-1</sup> )	$\lambda_{\text{em}}$ , nm	$\Delta\nu_{\text{St}}$ <sup>a</sup> , cm <sup>-1</sup>	$\Phi_{\text{F}}$ <sup>c</sup> , %	Solid	
						$\lambda_{\text{em}}$ , nm	$\Phi_{\text{F}}$ <sup>c</sup> , %
<b>2a</b>	Toluene	361 (2.65)	491	7334	75	499	6
	MeCN	356 (2.79), 260 (4.31)	612	11,750	34		
<b>2b</b>	Toluene	361 (0.81), 301 (0.75)	474	6604	3	463	23
	MeCN	350 (4.10)	627	12,622	13		
<b>2c</b>	Toluene	340 (6.25), 330 (6.40), 293 (8.09)	515 *, 467	9994 <sup>b</sup>	<1	421	26
	MeCN	318 (2.05), 291 (2.34), 255 (3.48)	550	13,264	1		
<b>2d</b>	Toluene	367 (2.54)	472	6062	63	512	<1
	MeCN	371 (2.58), 264 (2.52)	592	10,062	31		
<b>2e</b>	Toluene	360 (5.07)	474	6680	3	447	43
	MeCN	350 (1.84)	625	12,571	18		
<b>2f</b>	Toluene	340 (1.53), 329 (1.59)	412	5140	36	425	20
	MeCN	320 (0.91), 292 (1.52), 260 (2.10)	530	12,382	2		
<b>2g</b>	Toluene	371 (2.36)	502	7034	47	501	34
	MeCN	357 (2.39)	640	12,386	24		
<b>2h</b>	Toluene	381 (3.33)	473	5105	94	479	>95
	MeCN	371 (3.12), 269 (4.82)	615	10,694	25		
	Toluene	340 (5.02), 328 (4.97)	517, 434 *	6370 <sup>b</sup>	<1	416	8
	MeCN	318 (4.55)	560	13,589	35		

<sup>a</sup> Stokes shifts were calculated considering the lowest energetic absorption band. <sup>b</sup> Relative to the major emission peak (in bold). <sup>c</sup> Absolute quantum yield in the solid state was measured by the integrated sphere method. \* The major emission peak.

Based on the nature of substituent R<sup>1</sup> in the aryl fragment, we have outlined the grouping of [1,2,4]triazolo[4,3-*c*]quinazoline chromophores **2a–i** for the discussion of optical properties: Me-group (**2a–c**), MeO-group (**2d–f**) and CF<sub>3</sub>-group (**2e–h**); in each group of compounds, the substituent NR<sub>2</sub> in the biphenyl fragment was NEt<sub>2</sub>, NPh<sub>2</sub> or 9*H*-carbazol-9-yl.

The positions of the longest wavelength absorption bands of Et<sub>2</sub>N and Ph<sub>2</sub>N-containing fluorophores **2a**, **b**, **d**, **e**, **g**, **h** are observed in the UV region: 360–381 nm in toluene and 350–371 nm in MeCN (Table 1). The carbazolyl-derivatives **2c**, **2f** and **2i** are characterized by a blue-shifted (about 20–40 nm in toluene and 30–50 nm in MeCN) absorption band with respect to their diethylamino or diphenylamino counterparts, which is due to the decrease in conjugation length caused by the rigid structure of the carbazolyl unit. Notably, the profile of absorption spectra and positions of maxima in toluene are similar for compounds **2c**, **2f** and **2i** and are not influenced by the nature of substituent R<sup>1</sup> in the aryl fragment (Me, OMe or CF<sub>3</sub>), whereas the absorption band of CF<sub>3</sub>C<sub>6</sub>H<sub>4</sub>-containing triazoloquinazolines with a diethyl- or diphenyl-amino fragment (**2g** and **2h**, respectively) is bathochromically shifted with respect to the corresponding fluorophores **2a,d** and **2b,e** (Table 1).

Triazoloquinazolines **2a–i** have fluorescence emission maxima at 412–502 nm in toluene and 530–640 nm in MeCN, with quantum yields up to 94% (Table 1). We considered the influence of substituents R and R<sup>1</sup> on PL characteristics. For example, a red shift in emission maximum was observed in the order **2d**→**2a**→**2g** for diethylamino-containing **2a**, **2d** and **2g** both in toluene and MeCN solution (Supplementary Materials—Figures S20a and S21a), which can be explained by the decrease in electron-donating influence of the CH<sub>3</sub> group compared to MeO (compounds **2d** and **2a**) and by the increase in electron-withdrawing ability of the aryltriazol fragment due to the replacement of CH<sub>3</sub> with CF<sub>3</sub> (compounds **2a** and **2g**). For this set of compounds (**2a**, **2d** and **2g**), we

observed the attenuation of PL emission intensity when going from toluene to MeCN, which was probably caused by the reinforced charge transfer process in the excited state. On the contrary, the emission band of diphenylamino-containing fluorophores **2b**, **2e** and **2h** does not depend on the nature of the aryl unit at the triazole ring (Supplementary Materials—Figures S20b and S21b). The QY of (trifluoromethyl)phenyl-[1,2,4]triazolo[4,3-*c*]quinazoline **2h** appeared to be the strongest in both solvents ( $\Phi_F = 94\%$  in toluene), which clearly indicates that the trifluorophenyl group plays an essential role in the intense emission for  $NPh_2$ -containing derivatives **2b**, **e**, **h**. Fluorophores **2c**, **2f** and **2i** bearing the carbazolyl unit display the emission maxima at 530, 550 and 560 nm in MeCN and show the same dependence of emission wavelength on aryl fragment nature, **2f**→**2c**→**2i** (Supplementary Materials—Figure S21c) as their diethylamino counterparts. It is worth noting that derivatives **2c** ( $R^1 = CH_3$ ) and **2i** ( $R^1 = CF_3$ ) display a bimodal emission band in non-polar solvent (toluene) with a peak in high energy region at 467 and 434 nm, respectively, and at low energy, wavelengths at 515 and 517 nm, whereas compound **2f** ( $R^1 = OCH_3$ ) only shows the high energy band in toluene with a maximum at 412 nm (Supplementary Materials—Figure S20c). The bimodal emission can arise, for example, due to the existence of associates with solvents or aggregates. For the establishment of the exact reasons, additional studies will be conducted.

Along each series of quinazolines (Me-group, MeO-group, and  $CF_3$ -group), the carbazolyl-containing fluorophores **2c**, **2f** and **2i** demonstrate emissions in the highest energetic region in MeCN ( $\lambda_{max} = 550, 530$  and  $560$  nm, Table 1, Supplementary Materials—Figure S23), which agrees with the low electron-donating ability of the carbazol-9-yl unit. The introduction of  $NEt_2$  or  $NPh_2$  results in the bathochromically shifted emission band (compounds **2a**, **b**, **d**, **e**, **g**, **h**, Supplementary Materials—Figure S23).

The quinazoline-based fluorophores **2a–i** display an emission in the range of 416–512 nm in the solid state (powder), as shown in Table 1. The influence of the electron-donating substituent  $NR_2$  on the emission maximum is similar in each group of compounds; a blue shift is observed in the order  $NEt_2$ → $NPh_2$ →carbazol-9-yl. The quantum yield increases in the order  $NEt_2$ → $NPh_2$ , and obviously, the steric effect of a non-planar propeller-like configuration of the  $NPh_2$  group prevents molecules from packing via  $\pi$ - $\pi$  stacking and quenching [22–26]. (Figure 4, Supplementary Materials—Figure S24, Table 1). A very high quantum yield of the compound **2h** (>95%) should be noted.

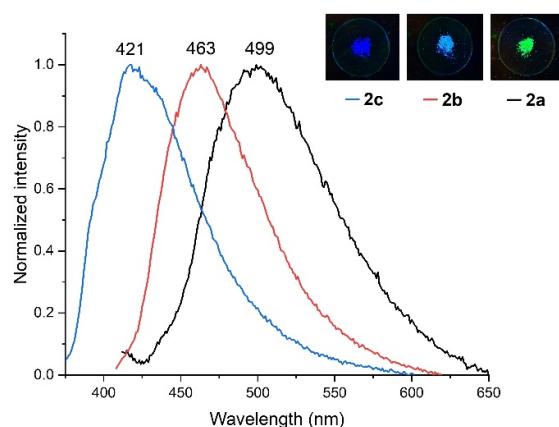


**Figure 4.** Normalized emission spectra of quinazolinones **2a–c** in solid state; inset: emission of compounds **2a–c** in solid state (powder). Photographs were taken in the dark upon irradiation with a hand-held UV lamp ( $\lambda_{em} = 366$  nm).

It is interesting to compare the triazolo-containing fluorophores **2a–i** with their 4-morpholinylquinazoline, 4-cyanoquinazoline or quinazolin-4-one counterparts containing the same 4'-amino[1,1'-biphenyl]-4-yl substituents [19,20]. We can conclude that the absorption maximum is not significantly influenced by the nature of the quinazoline core in the set of triazoloquinazoline, 4-morpholinylquinazoline and quinazolin-4-one, whereas

emission bands of compounds **2a–i** undergo a shift to longer wavelengths in all cases compared to their analogs. For example, compound **2a** demonstrates an emission maximum at 491 nm in toluene and 612 nm in MeCN, whereas 2-(4'-N,N-diethylamino[1,1'-biphenyl]-4-yl)quinazolin-4(3H)-one exhibits emissions with  $\lambda_{\max} = 450$  nm in toluene and 535 nm in MeCN [19], and 2-(4'-N,N-diethylamino[1,1'-biphenyl]-4-yl)-4-(morpholin-4-yl)quinazoline has  $\lambda_{\max} = 443$  nm in toluene and 554 nm in MeCN [20]), which confirms the reinforcement of interactions between the donor and acceptor part. Moreover, photophysical characteristics of **2a–i** differ considerably from those of cyano derivatives (for example, the absence of a shoulder in the red region of the absorption band, a higher quantum yield both in solution and solid state, etc. [19]). Notably, in the series of triazoloquinazolines **2**, the great bathochromic shift of the emission band is observed when the electron donor NR<sub>2</sub> group changes from NEt<sub>2</sub> to NPh<sub>2</sub> and further to carbazolyl (78–87 nm, Table 1), while for other types of fluorophores, the position of emission maximum is less dependent on NR<sub>2</sub>. This is probably because the presence of an aryl fragment in the triazole ring and the formation of a pincer-type structure prevents structure twisting, which leads to a more considerable and dependent correlation between the aryl donor group and emission maximum.

### 2.3. Effects of Solvent Polarity for **2a**, **d**, **g**, **h**

A study of luminescent properties in solvents of different polarity was performed for compounds **2a**, **2d**, **2g** and **2h** possessing high emission intensity in toluene ( $\Phi_F$  47–94%) and MeCN ( $\Phi_F$  24–34%) (Supplementary Materials—Tables S5–S8, Figure S25). The values of the emission maxima in different solvents are presented in Table 2. It has been shown that with increasing solvent polarity, the emission maximum of these chromophores underwent a red shift; the positive emission solvatochromism was observed. The most significant changes in the emission spectrum were noticed for compound **2a** ( $\lambda_{em} = 451$  nm in cyclohexane and  $\lambda_{em} = 648$  nm in methanol) (Figure 5a).

**Table 2.** Emission maxima of triazoloquinazolines **2a**, **d**, **g**, **h** in different solvents (excitation at longest wavelength absorption maximum) and parameters  $Z$  and  $E_T(30)$  for the chosen solvents.

Solvent	$Z$ , kcal/mol	$E_T(30)$ , kcal/mol	$\lambda_{em}$ , nm			
			<b>2a</b>	<b>2d</b>	<b>2g</b>	<b>2h</b>
Methanol	83.6	55.4	648	614	651	624
Acetonitrile	71.3	45.6	614	593	622	614
DMSO	71.1	45.1	632	616	643	624
DCM	64.7	40.7	555	531	565	554
THF	58.8	37.4	553	538	565	546
Toluene	-	33.9	489	478	500	482
Cyclohexane	-	30.9	451	424 *, 452	460	427, 468 *

\* The major emission peak.

We observed a rather large difference in the emission maxima upon passing from the least polar to the most polar solvent for other studied compounds **2d**, **g**, **h** as well (Supplementary Materials—Figure S25).

In addition, a mathematical analysis of the solvatochromic behavior was performed for the obtained compounds according to the typical procedure based on the Lippert–Mataga equation [27–29]. The data are presented in Table 3 and Figure 5b. The linearity of the plots was found to confirm the positive solvatochromic effect in all the cases. The obtained values of the difference between the dipole moments of the ground and excited states are in the range of 17.54–22.34 D, and the maximum value of 22.34 D is observed for [1,2,4]triazolo[4,3-*c*]quinazoline **2h** bearing a triphenylamine donor moiety and *p*-(trifluoromethyl)phenyl residue. Notably, the nature of the aryl substituent at the triazole ring has a significant

impact on the  $\Delta\mu$  value (the value increases in the order **2d**→**2a**→**2g**). Thus, a pronounced intramolecular charge transfer (ICT) process upon photoexcitation occurs in molecules **2a**, **d**, **g**, **h**.

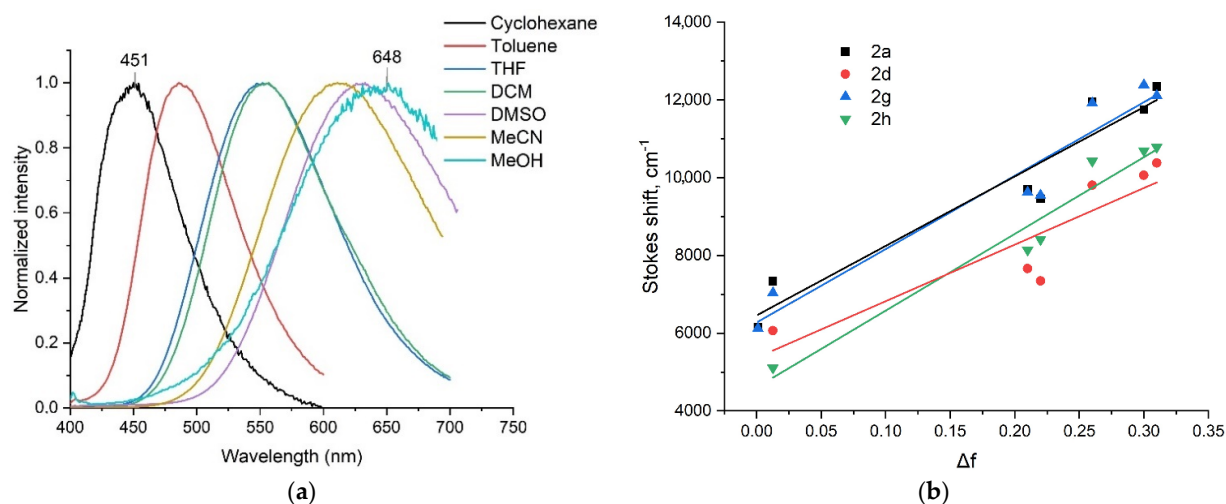


**Figure 5.** (a) Fluorescence spectra of compound **2a** in different solvents; (b) Lippert–Mataga plot of fluorophores **2a**, **2d**, **2g**, **2h** in cyclohexane (for **2a**, **2g**), toluene, THF, DCM, DMSO, MeCN and MeOH.

**Table 3.** Data from Lippert–Mataga plot for quinazolines **2a**, **2d**, **2g** and **2h**.

Comp.	Slopes	R <sup>2</sup>	<i>a</i> <sup>a</sup> , Å	$\Delta\mu$ , D
<b>2a</b>	17,874	0.93	4.71	19.26
<b>2d</b>	14,543	0.80	4.74	17.54
<b>2g</b>	18,893	0.94	4.78	20.24
<b>2h</b>	19,747	0.95	5.03	22.34

<sup>a</sup> *a*—Onsager radius, calculated following the literature [30].

We analyzed the dependence of the emission maxima bathochromic shift on the quantitative polarity criteria of the solvents used, in particular, according to Kosower [31,32] and Dimroth/Reichardt mathematical models [33,34]. In most cases, the longest wavelength emission maximum is observed for methanol, and the shortest value corresponds to cyclohexane. In general, the obtained values of the emission maxima correspond to the criteria for the polarity of solvents. Deviations occur for compound **2d** bearing the 4-methoxyphenyl substituent at position 3; in this case, the longest wavelength maximum is characteristic of DMSO, but a very small difference between the values of emission maxima in DMSO and methanol was noticed (2 nm). However, in all cases, the emission maximum in DMSO corresponds with the longer wavelength than in the case of acetonitrile (the difference is 3–24 nm), even though the difference between their polarity criteria is minimal.

The comparison of the obtained characteristics of **2a**, **2d**, **2g**, **2h** with the ones of some early published (hetero)aryl-substituted quinazolines allowed us to conclude that the condensation of an additional triazole ring led to a significant increase in  $\Delta\mu$  values. Thus, in the case of 2-(hetero)aryl-4-(4-aminophenyl)quinazolines [35], the obtained  $\Delta\mu$  values were 15.93–18.26 D. At the same time, it should be noted that the introduction of the aromatic substituent, instead of the heteroaromatic one at position C(2) of quinazoline, led to an increase in  $\Delta\mu$  values. For the group **2** compounds bearing aromatic substituents at the analogs position C(5), developed in the current work, the larger  $\Delta\mu$  values (up to 22.34 D) were determined.

It should be noted that the revealed positive solvatochromism phenomenon opens up a number of prospects for the application of novel group 2 compounds as potential candidates for designing fluorescent probes and as components for fluorescent and non-linear optical materials [36].

#### 2.4. Absorption and Fluorescence Behavior of Compounds **2b**, **2e** and **2h** in MeCN/water Mixture

Frequently, triphenylamino (TPA)-containing compounds demonstrate enhancement of emission intensity (AIEE) or inducement of emission (AIE) upon aggregation [22–26]. The X-ray data (Figure 3) obtained for quinazoline derivative **2e** bearing the TPA unit confirms the non-planar structure of the studied molecules. We considered the absorption and emission behavior of the compounds **2b**, **2e** and **2h** upon the addition of water based on the above-mentioned analysis on passing from MeCN solution to solid state. For this aim, we registered absorption and emission spectra of fluorophores **2b**, **2e** and **2h** (at  $c = 2 \times 10^{-6}$  M) in pure MeCN and in MeCN/water mixtures with various water fractions ( $f_w$ ); see Figure 6 and Supplementary Materials Figures S26–S28. Figure 6 demonstrates changes in fluorescence spectra of **2e** in MeCN and MeCN/water mixtures (a) and a plot of relative PL intensity ( $I/I_0$ ) and wavelength at emission maxima of **2e** versus the composition of the water fraction (b) at room temperature. After the first portion of H<sub>2</sub>O, we observe a dramatic attenuation of emission intensity and red shift of the band. After 70vol% of water, the band shifts toward the blue region with the regeneration of intensity, and the strongest emission was measured at 80vol% of water. Other compounds (**2b** and **2h**) demonstrate similar changes in emission spectra. These changes are typical for luminogens with a rotatable donor–acceptor (D–A) structure, which possess two excited states: a locally excited (LE) state and a twisted intramolecular charge transfer (TICT) state. When the polarity of media increases (upon the addition of water), the TICT state becomes dominant, leading to red-shifted emission and the quenching of intensity. Further addition of water most likely led to the formation of aggregates that are less polar than initial single molecules, and this phenomenon resulted in blue-shifted emission. The intensity restores due to the restriction of rotation in the TPA group and phenylene moieties and the reducing non-radiative transitions. Thus, compounds **2b**, **2e** and **2h** exhibited aggregation-induced emission enhancement to some extent.

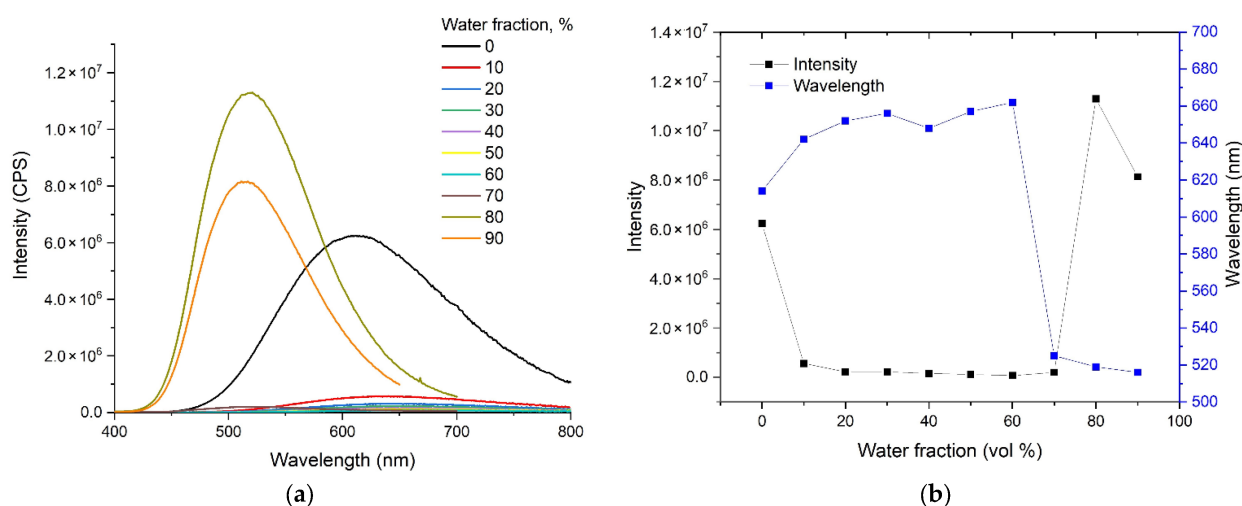


**Figure 6.** (a) The fluorescence spectra of **2e** in MeCN and MeCN/water mixtures with different water fractions ( $f_w$ ); (b) a plot of relative PL intensity ( $I/I_0$ ) and wavelength at emission maxima of **2e** versus the composition of the water fraction (vol %).  $T = 23$  °C.

As for UV/vis spectra for quinazolines **2b**, **2e** and **2h**, we observed that the absorption band registered at 90%, 80% and 70% water fraction, respectively, was bathochromically shifted compared to pure MeCN, which can be ascribed to the formation of J-type aggre-

gates with head-to-tail arrangement (Supplementary Materials—Figures S26c, S27a and S28c) [37–39].

Additionally, we carried out a time-resolved fluorescence study of quinazolines **2b**, **2e** and **2h** in a pure MeCN and MeCN/water mixture (Supplementary Materials—Figures S26d, S27b, S28d and S29–S31); fluorescence lifetimes were estimated to complete the photophysical characterization of the fluorophores. The lifetime of compound **2b** is fitted with bi-exponential decay with an average lifetime of 2.38 ns, whereas compounds **2e** and **2h** are characterized by mono-exponential decay curves and lifetimes of 3.17 and 2.46 ns, respectively (Supplementary Materials—Table S9). Fluorescence decay profiles of aggregated quinazolines at the highest emission intensity are fitted with three-exponential decay. Notably, the highest fractional contribution is different for all three compounds. While for *p*-tolyl-containing fluorophores, the highest fractional contribution at  $\tau_2 = 2.96$  ns was detected, for their methoxy counterparts, it was observed at  $\tau_1 = 7.76$  ns. On the contrary, the introduction of an electron-withdrawing  $\text{CF}_3$  group is reflected in the increased contribution of shorter time,  $\tau_3 = 1.36$  ns (Supplementary Materials—Table S9). Generally, the average lifetimes of compounds **2b** and **2e** increase (for **2e** more considerable) and were found to be 3.57 and 7.72 ns, respectively, while  $\tau_{\text{av}}$  of **2h** decreases by 1.36 ns in the MeCN/water mixture with respect to pure MeCN.

### 2.5. Absorption and Fluorescence Behavior of Compounds **2e** and **2h** in Acidic Media

Because triazoloquinazolines **2a–i** bear nitrogen atoms that can bind with proton, we intend to investigate the absorption and fluorescence sensory properties of some samples toward acid. For the experiment, we have chosen quinazoline **2e**, containing an electron-donating *p*-methoxy substituent that reinforces the basicity of the triazole ring. On the contrary, the *p*-(trifluoromethyl)phenyl residue (compound **2h**) attenuates the basicity of the nitrogen atoms, and this derivative possesses the strongest fluorescence intensity in pure toluene, as was mentioned above. Nevertheless, both compounds demonstrate similar behavior upon the addition of TFA to toluene solution under UV light and daylight by the naked eye (Supplementary Materials—Figure S32). The color of the solution turns from colorless to yellow (for **2e**) or orange (for **2h**) under daylight. The emission changes from dark blue or blue to orange. Both compounds demonstrate the reversibility of absorption and emission upon the consecutive addition of TFA and TEA. The titration experiment shows that the longwave absorption peak is red-shifted (from 360 to 372 nm in the case of **2e** and from 381 to 389 nm for **2h**), forming a tail-shaped band in the region of 380–440 nm and 420–460 nm, respectively, upon the addition of an excess of TFA (Figures 7a and S33a). The emission behaviour of fluorophore **2e** is more interesting in acidic media, and the changes are observed at a lower equivalent than that of compound **2h** (Figure 7). After the first portion of acid, we observe the bathochromic shift of the emission band and gradual enhancement of emission intensity. When 200 equivalents of TFA were added, the fluorescent intensity reached the highest value, and the peak at 528 nm appeared. The subsequent addition of acid resulted in the attenuation of intensity and further red shift by 540 nm at 500 eq of acid.

The emission band of compound **2h** shifts to the red region with a gradual attenuation of intensity (Supplementary Materials—Figure S33b). The appearance of red-shifted absorption and emission bands in both cases can be associated with the reinforcement of electron-withdrawing strength of the triazoloquinazoline core due to the protonation of the nitrogen atom resulting in a stronger interaction of acceptor and donor units compared to neutral molecules. Therefore, significant acidochromic behavior was observed for compounds **2e**, **h**. We can suppose that changes in emission intensity (enhancement or quenching) of compounds **2e** and **2h** might be due to intramolecular photo-induced electron transfer (PET) or photo-induced proton transfer [40], and the elucidation of the exact interaction mechanism of the analyte with TFA is under progress.

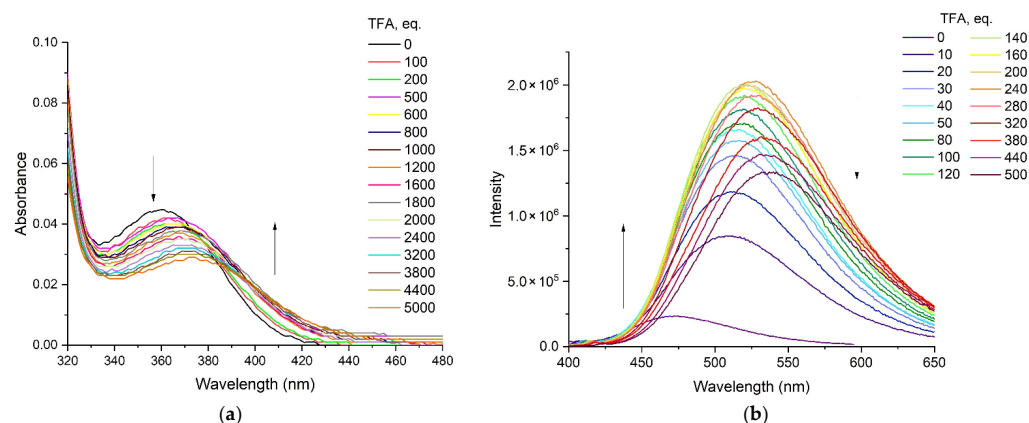


**Figure 7.** Changes in absorption (a) and emission (b) spectra of the toluene solution ( $c = 10^{-5}$  M) of **2e** upon gradual addition of TFA.

### 2.6. Quantum-Chemical Calculations

Furthermore, we performed the DFT calculations of quinazolines **2a–i** in the gas phase at the B3LYP/6–311 G\* level using the Orca 4.0.1 software package [41–45] and conducted the chemical optimization on their energy levels based on DFT/B3LYP/6-31G (d,p) using Gaussian 09. The distribution plots of the HOMOs and LUMOs, as well as energy levels and energy gaps, are presented in Figure 7. Notably, the distribution plots of the HOMOs of diethylamino-containing fluorophores **2a** and **2d** are distinctly different from other counterparts. For molecules **2a** and **2d**, the HOMO electrons are mainly distributed on the 3-aryltriazolo[4,3-*c*]quinazoline fragment, which shows the considerable influence of the electronic nature of the substituent at the para-position of the phenylene ring. For compounds **2b**, **c**, **e–i**, the HOMO electrons are mainly located at the electron-donating arylamino unit, with the phenylene ring less involved in carbazolyl-derivatives **2c**, **2f** and **2i**, which confirms weaker  $\pi$ -conjugation of these molecules due to twisting of the rigid carbazolyl fragment and is consistent with photophysical data. The LUMOs plots are similar for all the compounds **2a–i** (Figure 8); electrons are distributed on the 5-(biphenyl-4-yl)-[1,2,4]triazolo[4,3-*c*]quinazoline framework. In general, the value of the energy gap decreases in each set of compounds bearing the same aminoaryl group with an increase in electron-withdrawing ability of the aryl substituent at position C(3). It is worth noting that energy levels of triazolo[4,3-*c*]quinazolines are closer to that of previously described 2-biphenylquinazolin-4(3*H*)-one derivatives than to ones for 4-morpholinyl or 4-cyano counterparts [19,20].

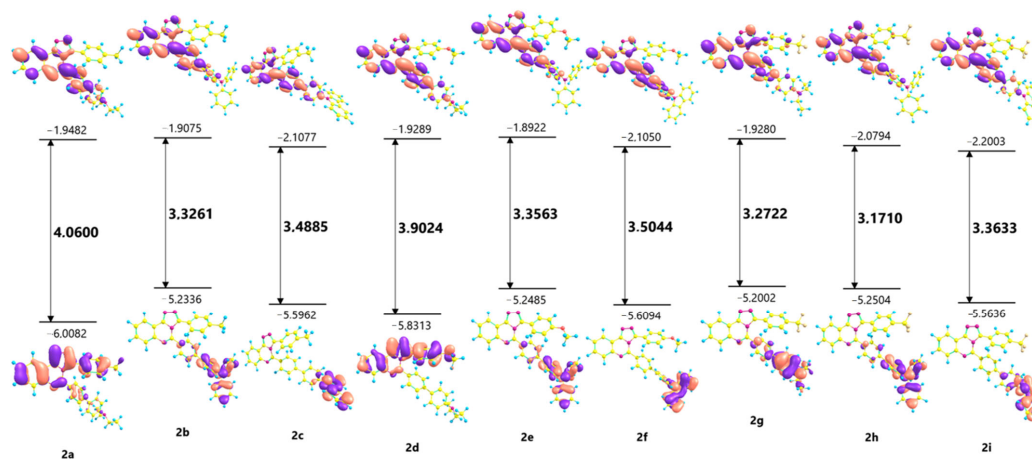


**Figure 8.** Optimized molecular structures and molecular orbitals of the HOMO and LUMO levels, energy gaps and electron cloud distribution of triazoloquinazolines **2a–i**.

Obviously, different electronic distributions on HOMO and LUMO levels for compounds **2a–i** confirm the intense intramolecular charge transfer (ICT) process, which is consistent with solvatochromic studies for the considered compounds.

### 3. Experimental Methods

#### 3.1. General Information

Unless otherwise indicated, all common reagents and solvents were used from commercial suppliers without further purification. Melting points were determined on Boetius-combined heating stages.  $^1\text{H}$  NMR and  $^{13}\text{C}$  NMR spectra were recorded at room temperature at 400 and 100 MHz, respectively, on a Bruker DRX-400 spectrometer (Bruker, Rheinstetten, Germany). Hydrogen chemical shifts were referenced to the hydrogen resonance of the corresponding solvent (DMSO- $d_6$ ,  $\delta = 2.50$  ppm or  $\text{CDCl}_3$ ,  $\delta = 7.26$  ppm). Carbon chemical shifts were referenced to the carbon resonances of the solvent (DMSO- $d_6$ ,  $\delta = 39.5$  ppm  $\text{CDCl}_3$ ,  $\delta = 77.2$  ppm). Peaks are labelled as singlet (s), doublet (d), triplet (t), quartet (q) and multiplet (m). Mass spectra were recorded on the SHIMADZU GCMS-QP2010 Ultra instrument (Shimadzu, Duisburg, Germany) with the electron ionization (EI) of the sample. Microanalyses (C, H, N) were performed using the Perkin–Elmer 2400 elemental analyser (Perkin–Elmer, Waltham, MA, USA).

#### 3.2. Photophysical Characterization

UV/vis absorption spectra were recorded on the Shimadzu UV-1800 Spectrophotometer (Shimadzu, Duisburg, Germany) using quartz cells with 1 cm path length at room temperature. Emission spectra were measured on the Horiba FluoroMax-4 (HORIBA Ltd., Kyoto, Japan) at room temperature using quartz cells with 1 cm path length. The fluorescence quantum yield of the target compounds in solution and solid state were measured by using the Integrating Sphere Quanta- $\phi$  of the Horiba-Fluoromax-4. Time-resolved fluorescence measurements were carried out using time-correlated single-photon counting (TCSPC) with a nanosecond LED ( $\lambda = 370$  nm).

#### 3.3. Crystallography

The single crystal (light yellow block of  $0.38 \times 0.24 \times 0.20$ ) of compound **2a** and the single crystal (yellow block of  $0.43 \times 0.35 \times 0.28$ ) of compound **2e** were used for X-ray analysis. Structural studies were performed using equipment available in the Collaborative Access Center “Testing Center of Nanotechnology and Advanced Materials” at the Mikheev Institute of Metal Physics, Ural Branch, Russian Academy of Sciences. The X-ray diffraction analysis was performed at room temperature on Rigaku OD XtaLAB Synergy-S diffractometer (Rigaku Oxford Diffraction, Tokyo, Japan). Using Olex2 [46], the structure was solved with the ShelXT structure solution program using Intrinsic Phasing and refined with the ShelXL [47] refinement package using full-matrix least squares minimization. All non-hydrogen atoms were refined in an anisotropic approximation; the H-atoms were placed in the calculated positions and refined isotropically in the “rider” model. Crystal data for **2a**  $\text{C}_{32}\text{H}_{29}\text{N}_5$ ,  $M = 483.60$ , monoclinic,  $a = 12.64210(10)$  Å,  $b = 11.96340(10)$  Å,  $c = 17.2021(2)$  Å,  $\alpha = 90^\circ$ ,  $\beta = 103.4260(10)^\circ$ ,  $\gamma = 90^\circ$ ,  $V = 2530.59(4)$  Å<sup>3</sup>, space group  $P2_1/c$ ,  $Z = 4$ ,  $\mu(\text{Mo K}\alpha) = 0.077$  mm<sup>-1</sup>. On the angles  $4.75 < 2\theta < 52.744^\circ$ , 5154 reflections were measured, 3812 unique ( $R_{\text{int}} = 0.1062$ ), which were used in all calculations. Goodness to fit at  $F^2$  1.151; the final  $R_1 = 0.1290$ ,  $wR_2 = 0.2736$  (all data) and  $R_1 = 0.0770$ ,  $wR_2 = 0.2018$  ( $I > 2\sigma(I)$ ). Largest diff. peak and hole 0.21 and  $-0.23$  eÅ<sup>-3</sup>.

Crystal data for **2e**  $\text{C}_{40}\text{H}_{29}\text{N}_5$ ,  $M = 595.68$ , orthorhombic,  $a = 76.1636(13)$  Å,  $b = 17.3954(3)$  Å,  $c = 9.57464(12)$  Å,  $\alpha = 90^\circ$ ,  $\beta = 90^\circ$ ,  $\gamma = 90^\circ$ ,  $V = 12685.4(4)$  Å<sup>3</sup>, space group  $Fdd2$ ,  $Z = 16$ ,  $\mu(\text{Mo K}\alpha) = 0.077$  mm<sup>-1</sup>. On the angles  $2.14 < 2\theta < 29.48^\circ$ , 8203 reflections were measured, 3575 unique ( $R_{\text{int}} = 0.2091$ ), which were used in all calculations. Goodness to fit at  $F^2$  0.975; the final  $R_1 = 0.1695$ ,  $wR_2 = 0.2165$  (all data) and  $R_1 = 0.0605$ ,  $wR_2 = 0.1491$  ( $I > 2\sigma(I)$ ). Largest diff. peak and hole 0.18 and  $-0.20$  eÅ<sup>-3</sup>.

The results of the X-ray diffraction analysis for compounds **2a** and **2e** were deposited with the Cambridge Crystallographic Data Centre (CCDC 2218321 for **2a** and CCDC 2217179 for **2e**). The data are free and can be accessed at [www.ccdc.cam.ac.uk](http://www.ccdc.cam.ac.uk) (accessed on 8 November 2022 for **2a** and 3 November 2022 for **2e**).

### 3.4. General Procedures of Suzuki Cross-Coupling

To the mixture of bromo derivative **1a–c** (0.65 mmol) in toluene (10 mL), the corresponding boronic acid or boronic acid pinacol ester (0.70 mmol), PdCl<sub>2</sub>(PPh<sub>3</sub>)<sub>2</sub> (46 mg, 65 μmol), PPh<sub>3</sub> (34 mg, 130 μmol), saturated solution of K<sub>2</sub>CO<sub>3</sub> (3.7 mL) and EtOH (3.7 mL) were added. The mixture was stirred at 85 °C for 7–20 h in argon atmosphere in a round-bottom pressure flask. The reaction mixture was cooled. After cooling, the organic layer was separated, washed sequentially with EtOAc (10 mL) and H<sub>2</sub>O (10 mL), dried over Na<sub>2</sub>SO<sub>4</sub>, and the organic layer was evaporated at reduced pressure. The product was isolated by gradient column chromatography on silica gel, a mixture of hexane and ethyl acetate was used as an eluent.

**5-(4'-Diethylamino-[1,1']-biphenyl-4-yl)-3-(*p*-tolyl)-[1,2,4]triazolo[4,3-*c*]quinazoline (2a).** Yellow powder, yield 25%; mp 195–197 °C; <sup>1</sup>H NMR (CDCl<sub>3</sub>, 400 MHz) δ 1.21 (6H, t, <sup>3</sup>J = 7.2 Hz, 2CH<sub>3</sub>), 2.24 (3H, s, CH<sub>3</sub>), 3.42 (4H, q, <sup>3</sup>J = 7.2 Hz, 2CH<sub>2</sub>), 6.74 (2H, d, <sup>3</sup>J = 8.3 Hz, 2CH<sub>phenylene</sub>), 6.91 (2H, d, <sup>3</sup>J = 7.8 Hz, 2CH<sub>phenylene</sub>), 7.08 (2H, d, <sup>3</sup>J = 7.8 Hz, 2CH<sub>phenylene</sub>), 7.23–7.30 (4H, m, 4CH<sub>phenylene</sub>), 7.36 (2H, d, <sup>3</sup>J = 8.3 Hz, 2CH<sub>phenylene</sub>), 7.73 (1H, m, CH<sub>quinaz</sub>), 7.81 (1H, m, CH<sub>quinaz</sub>), 8.04 (1H, d, <sup>3</sup>J = 8.1 Hz, m, CH<sub>quinaz</sub>), 8.76 (1H, d, <sup>3</sup>J = 7.8 Hz, m, CH<sub>quinaz</sub>); <sup>13</sup>C NMR (CDCl<sub>3</sub>, 100 MHz) δ 12.7 (2CH<sub>3</sub>), 21.4 (CH<sub>3</sub>), 44.5 (2CH<sub>2</sub>), 111.9, 116.5, 123.6, 125.0, 125.3, 126.7, 128.1, 128.4, 128.6, 129.1, 129.3, 129.5, 129.7, 131.8, 139.5, 141.3, 143.7, 146.1, 147.8, 149.3, 150.0; EIMS *m/z* 484 [M + 1]<sup>+</sup> (26), 483 [M]<sup>+</sup> (69), 469 (37), 468 (100) 234 (21); anal. C 79.47, H 14.48, N 8.94%, calcd for C<sub>32</sub>H<sub>29</sub>N<sub>5</sub> (483.62) C 79.40, H 6.12, N 14.11%.

**5-(4'-Diphenylamino-[1,1']-biphenyl-4-yl)-3-(*p*-tolyl)-[1,2,4]triazolo[4,3-*c*]quinazoline (2b).** Beige powder, yield 48%; mp 205–207 °C; <sup>1</sup>H NMR (CDCl<sub>3</sub>, 400 MHz) δ 2.24 (3H, s, CH<sub>3</sub>), 6.93 (2H, d, <sup>3</sup>J = 7.7 Hz, 2CH<sub>phenylene</sub>), 7.09–7.18 (10H, m), 7.28–7.36 (10H, m), 7.76 (1H, m, CH<sub>quinaz</sub>), 7.84 (1H, m, CH<sub>quinaz</sub>), 8.06 (1H, d, <sup>3</sup>J = 8.0 Hz, CH<sub>quinaz</sub>), 8.78 (1H, d, <sup>3</sup>J = 7.9 Hz, CH<sub>quinaz</sub>); <sup>13</sup>C NMR (100 MHz, CDCl<sub>3</sub>) δ 21.4 (CH<sub>3</sub>), 116.6, 123.5, 123.6, 124.9, 125.0, 126.0, 127.9, 128.4, 128.6, 129.3, 129.4, 129.5, 129.7, 130.6, 131.9, 133.7, 139.5, 141.3, 143.1, 145.8, 147.6, 148.1, 149.2, 150.0; EIMS *m/z* 580 [M + 1]<sup>+</sup> (44), 579 [M]<sup>+</sup> (100), 578 (11), 289 (17); anal. C 82.88, H 5.04, N 12.08%, calcd for C<sub>40</sub>H<sub>29</sub>N<sub>5</sub> (579.71) C 82.88, H 5.01, N 12.00%.

**5-(4'-(9H-Carbazol-9-yl)-[1,1']-biphenyl-4-yl)-3-(*p*-tolyl)-[1,2,4]triazolo[4,3-*c*]quinazoline (2c).** After cooling, the reaction mixture was filtered and washed with hexane. Colourless powder, yield 65%; mp 236–238 °C; <sup>1</sup>H NMR (CDCl<sub>3</sub>, 400 MHz) δ 2.27 (3H, s, CH<sub>3</sub>), 6.97 (2H, d, <sup>3</sup>J = 7.8 Hz, 2CH<sub>phenylene</sub>), 7.12 (2H, d, <sup>3</sup>J = 7.8 Hz, 2CH<sub>phenylene</sub>), 7.32 (2H, m, 2CH<sub>carbaz</sub>), 7.42–7.50 (10H, m), 7.69 (4H, m), 7.77 (1H, m, CH<sub>quinaz</sub>), 7.84 (1H, m, CH<sub>quinaz</sub>), 8.07 (1H, d, <sup>3</sup>J = 8.1 Hz, CH<sub>quinaz</sub>), 8.17 (2H, d, <sup>3</sup>J = 7.8 Hz, 2CH<sub>carbaz</sub>), 8.80 (1H, d, <sup>3</sup>J = 7.8 Hz, CH<sub>quinaz</sub>); <sup>13</sup>C NMR (100 MHz, CDCl<sub>3</sub>) δ 21.5 (CH<sub>3</sub>), 109.9, 116.6, 120.3, 120.6, 123.6, 123.7, 125.0, 126.2, 126.6, 127.6, 128.5, 128.6, 128.7, 129.4, 129.6, 129.8, 131.6, 132.0, 137.8, 139.2, 139.6, 140.9, 141.2, 142.6, 145.6, 149.1, 150.0; EIMS *m/z* 579 [M + 2]<sup>+</sup> (10), 578 [M + 1]<sup>+</sup> (45), 577 [M]<sup>+</sup> (100), 344 (11), 288 (24), 241 (11), 102 (17), 88 (12), 77 (14), 57 (10), 44 (39), 43 (28), 41 (13); anal. C 83.17, H 4.71, N 12.12%, calcd for C<sub>40</sub>H<sub>27</sub>N<sub>5</sub> (577.69) C 83.12, H 4.11, N 12.15%.

**5-(4'-Diethylamino-[1,1']-biphenyl-4-yl)-3-(4-methoxyphenyl)-[1,2,4]triazolo[4,3-*c*]quinazoline (2d).** After cooling, the reaction mixture was filtered and washed with hexane. The product was additionally recrystallized from CH<sub>2</sub>Cl<sub>2</sub>/hexane mixture. Yellow powder, yield 29%; mp 189–191 °C; <sup>1</sup>H NMR (CDCl<sub>3</sub>, 400 MHz) δ 1.21 (6H, t, <sup>3</sup>J = 7.0 Hz, 2CH<sub>3</sub>), 3.41 (4H, q, <sup>3</sup>J = 7.0 Hz, 2CH<sub>2</sub>), 3.63 (3H, s, OCH<sub>3</sub>), 6.62 (2H, d, <sup>3</sup>J = 8.5 Hz, 2CH<sub>phenylene</sub>), 6.74 (2H, d, <sup>3</sup>J = 8.5 Hz, 2CH<sub>phenylene</sub>), 7.11 (2H, d, <sup>3</sup>J = 8.1 Hz, 2CH<sub>phenylene</sub>), 7.8 (4H,

m, 4CH<sub>phenylene</sub>), 7.37 (2H, d, <sup>3</sup>J = 8.1 Hz, 2CH<sub>phenylene</sub>), 7.73 (1H, m, CH<sub>quinaz</sub>), 7.78 (1H, m, CH<sub>quinaz</sub>), 8.03 (1H, d, <sup>3</sup>J = 7.3, CH<sub>quinaz</sub>), 8.75 (1H, d, <sup>3</sup>J = 7.2, CH<sub>quinaz</sub>); <sup>13</sup>C NMR (100 MHz, CDCl<sub>3</sub>) 12.8 (2CH<sub>3</sub>), 44.8 (2CH<sub>2</sub>), 55.5 (OCH<sub>3</sub>), 112.0, 113.4, 116.6, 120.2, 123.5, 125.3, 126.7, 128.1, 128.4, 129.1, 129.4, 129.5, 131.2, 131.8, 141.3, 143.6, 146.1, 147.8, 149.1, 150.0, 160.6; EIMS *m/z* 500 [M + 1]<sup>+</sup> (32), 499 [M]<sup>+</sup> (85), 485 (34), 484 (100), 242 (47), 228 (11), 207 (10); anal. C 76.93, H 5.85, N 14.02%, calcd for C<sub>32</sub>H<sub>29</sub>N<sub>5</sub>O (499.62) C 76.90, H 5.87, N 14.10%.

**5-(4'-Diphenylamino-[1,1']-biphenyl-4-yl)-3-(4-methoxyphenyl)-[1,2,4]triazolo[4,3-c]quinazoline (2e).** The product was additionally recrystallized from CH<sub>2</sub>Cl<sub>2</sub>/hexane mixture. Pale yellow powder, yield 51%; mp 242–244 °C; <sup>1</sup>H NMR (CDCl<sub>3</sub>, 400 MHz) δ 3.64 (3H, s, OCH<sub>3</sub>), 6.62 (2H, d, <sup>3</sup>J = 6.6 Hz, 2CH<sub>phenylene</sub>), 7.02–7.16 (10H, m), 7.26–7.36 (10H, m), 7.74 (1H, m, CH<sub>quinaz</sub>), 7.82 (1H, m, CH<sub>quinaz</sub>), 8.04 (1H, d, <sup>3</sup>J = 8.2 Hz, CH<sub>quinaz</sub>), 8.76 (1H, d, <sup>3</sup>J = 7.7 Hz, CH<sub>quinaz</sub>); <sup>13</sup>C NMR (100 MHz, CDCl<sub>3</sub>) δ 55.4 (OCH<sub>3</sub>), 113.5, 116.6, 120.2, 123.5, 123.6, 124.8, 126.0, 127.9, 128.4, 129.3, 129.5, 129.5, 130.6, 131.2, 131.9, 133.7, 141.2, 143.0, 145.8, 147.6, 148.1, 149.0, 149.9, 160.6; EIMS *m/z* 597 [M + 2]<sup>+</sup> (10), 596 [M + 1]<sup>+</sup> (45), 595 [M]<sup>+</sup> (100), 298 (20); anal. C 80.65, H 4.91, N 11.76%, calcd for C<sub>40</sub>H<sub>29</sub>N<sub>5</sub>O (595.71) C 89.90, H 4.77, N 11.44%.

**5-(4'-(9H-Carbazol-9-yl)-[1,1']-biphenyl-4-yl)-3-(4-methoxyphenyl)-[1,2,4]triazoloquinazoline (2f).** After cooling, the reaction mixture was filtered and washed with hexane. The product was additionally recrystallized from DMSO. Grey powder, yield 38%; mp 277–279 °C; <sup>1</sup>H NMR (DMSO-*d*<sub>6</sub>, 400 MHz) δ 3.64 (3H, s, OCH<sub>3</sub>), 6.68 (2H, d, <sup>3</sup>J = 8.5 Hz, 2CH<sub>phenylene</sub>), 7.17 (2H, d, <sup>3</sup>J = 8.6 Hz, 2CH<sub>phenylene</sub>), 7.31 (2H, m, 2CH<sub>carbaz</sub>), 7.42–7.50 (m, 8H), 7.74 (2H, d, <sup>3</sup>J = 8.2 Hz, 2CH<sub>phenylene</sub>), 7.80–7.86 (3H, m), 7.91 (1H, m, CH<sub>quinaz</sub>), 8.04 (1H, d, <sup>3</sup>J = 8.0 Hz, CH<sub>quinaz</sub>), 8.24 (2H, m, 2CH<sub>carbaz</sub>), 8.63 (1H, d, <sup>3</sup>J = 7.8 Hz, CH<sub>quinaz</sub>); <sup>13</sup>C NMR (100 MHz, CDCl<sub>3</sub>) δ 55.4(OCH<sub>3</sub>), 109.9, 113.5, 116.6, 120.2, 120.3, 120.6, 123.6, 123.7, 126.2, 126.6, 127.6, 128.5, 128.7, 129.4, 129.7, 131.3, 131.6, 131.9, 137.8, 139.2, 140.9, 141.2, 142.5, 145.6, 148.9, 149.9, 160.6; EIMS *m/z* 594 [M + 1]<sup>+</sup> (44), 593 [M]<sup>+</sup> (100), 344 (16), 319 (14), 296 (30), 241 (17), 223 (12), 166 (17), 140 (12), 102 (12), 88 (17), 55 (16), 44 (32), 43 (38), 42 (19), 41 (11), 39 (17); anal. C 80.68, H 4.33, N 11.97%, calcd for C<sub>40</sub>H<sub>29</sub>N<sub>5</sub>O (593.69) C 80.92, H 4.58, N 11.80%.

**5-(4'-Diethylamino-[1,1']-biphenyl-4-yl)-3-(4-(trifluoromethyl)phenyl)-[1,2,4]triazoloquinazoline (2g).** The product was additionally recrystallized from CH<sub>2</sub>Cl<sub>2</sub>/hexane mixture. Yellow powder, yield 46%; mp 202–204 °C; <sup>1</sup>H NMR (CDCl<sub>3</sub>, 400 MHz) δ 1.21 (6H, t, <sup>3</sup>J = 7.1 Hz, 2CH<sub>3</sub>), 3.41 (4H, q, <sup>3</sup>J = 7.1 Hz, 2CH<sub>2</sub>), 6.72 (2H, d, <sup>3</sup>J = 7.4 Hz, 2CH<sub>phenylene</sub>), 7.30–7.42 (10H, m), 7.76 (1H, m, CH<sub>quinaz</sub>), 7.84 (1H, m, CH<sub>quinaz</sub>), 8.06 (1H, d, <sup>3</sup>J = 8.1 Hz, CH<sub>quinaz</sub>), 8.77 (1H, d, <sup>3</sup>J = 7.9 Hz, CH<sub>quinaz</sub>); <sup>19</sup>F NMR (CDCl<sub>3</sub>, 376 MHz) δ –62.73 (3F, s, CF<sub>3</sub>); <sup>13</sup>C NMR (100 MHz, CDCl<sub>3</sub>) δ 12.7 (2C, 2CH<sub>3</sub>), 44.5 (2C, 2CH<sub>2</sub>), 111.9, 116.3, 123.6 (1C, q, <sup>1</sup>J<sub>CF</sub> = 272.5 Hz, CF<sub>3</sub>), 123.7, 124.7 (2C, q, <sup>3</sup>J<sub>CF</sub> = 3.7 Hz, C<sub>6</sub>H<sub>5</sub>CF<sub>3</sub>), 125.6, 126.2, 128.1, 128.3, 128.5, 128.9, 129.2, 129.3, 129.4, 130.0, 130.2, 131.2, 131.5, 131.7, 132.2, 141.4, 144.5, 145.5, 147.9, 148.0, 150.6; EIMS *m/z* 538 [M + 1]<sup>+</sup> (30), 537 [M]<sup>+</sup> (78), 523 (36), 522 (100), 465 (12), 390 (11), 261 (25), 176 (10), 161 (12), 146 (12), 49 (12); anal. C 71.50, H 4.88, N 13.03%, calcd for C<sub>32</sub>H<sub>26</sub>F<sub>3</sub>N<sub>5</sub> (537.59) C 71.40, H 4.98, N 13.00%.

**5-(4'-Diphenylamino-[1,1']-biphenyl-4-yl)-3-(4-(trifluoromethyl)phenyl)-[1,2,4]triazoloquinazoline (2h).** Yellow powder, yield 64%; mp 197–199 °C; <sup>1</sup>H NMR (CDCl<sub>3</sub>, 400 MHz) δ 7.08 (2H, m, 2H<sub>phenyl</sub>), 7.14–7.21 (6H, m, 4H<sub>phenyl</sub>, 2H<sub>phenylene</sub>), 7.27–7.33 (4H, m, 4CH<sub>phenyl</sub>), 7.61 (2H, d, <sup>3</sup>J = 6.5 Hz, 2CH<sub>phenylene</sub>), 7.76 (1H, m, CH<sub>quinaz</sub>), 7.80 (2H, d, <sup>3</sup>J = 8.1 Hz, 2H<sub>phenylene</sub>), 7.85 (2H, d, <sup>3</sup>J = 8.0 Hz, 2H<sub>phenylene</sub>), 7.90 (1H, m, CH<sub>quinaz</sub>), 8.17 (1H, d, <sup>3</sup>J = 8.1 Hz, CH<sub>quinaz</sub>), 8.56 (d, 2H, <sup>3</sup>J = 8.0 Hz, 2H<sub>phenylene</sub>), 8.67 (1H, d, <sup>3</sup>J = 7.9 Hz, CH<sub>quinaz</sub>), 8.75 (2H, d, <sup>3</sup>J = 8.1 Hz, 2H<sub>phenylene</sub>); <sup>19</sup>F NMR (CDCl<sub>3</sub>, 376 MHz) δ –62.73 (3F, s, CF<sub>3</sub>); <sup>13</sup>C NMR (100 MHz, CDCl<sub>3</sub>) δ 117.4, 123.5, 123.6, 123.9, 124.3 (1C, q, <sup>1</sup>J<sub>CF</sub> = 271.7 Hz, CF<sub>3</sub>), 124.9, 125.8, 125.9, 126.6, 128.1 (2C, q, <sup>3</sup>J<sub>CF</sub> = 3.7 Hz, C<sub>6</sub>H<sub>5</sub>CF<sub>3</sub>), 128.5, 129.0, 129.5, 130.0, 131.1, 132.1, 132.4, 133.6, 133.9, 143.2, 144.0, 146.3, 147.7, 148.2, 153.3, 162.8; EIMS *m/z* 635 [M + 2]<sup>+</sup> (14), 634 [M + 1]<sup>+</sup> (55), 633 [M]<sup>+</sup> (100), 318 (10), 317 (34), 231 (14), 218 (13), 167

(21), 166 (15), 77 (19); anal. C 75.82, H 4.14, N 11.05%, calcd for C<sub>40</sub>H<sub>26</sub>F<sub>3</sub>N<sub>5</sub> (633.68) C 75.72, H 4.18, N 10.98%.

**5-(4'-(9H-Carbazol-9-yl)-[1,1']-biphenyl-4-yl)-3-(4-(trifluoromethyl)phenyl)-[1,2,4]triazolo[4,3-c]quinazoline (2i).** After cooling, the reaction mixture was filtered and washed with hexane. Grey powder, yield 50%; mp 305–307 °C; <sup>1</sup>H NMR (CDCl<sub>3</sub>, 400 MHz) δ 7.32 (2H, m, 2CH<sub>carbaz</sub>), 7.39–7.49 (12H, m), 7.69 (4H, m), 7.81 (1H, m, CH<sub>quinaz</sub>), 7.88 (1H, t, CH<sub>quinaz</sub>), 8.10 (1H, d, <sup>3</sup>J = 8.2 Hz, CH<sub>quinaz</sub>), 8.17 (2H, d, <sup>3</sup>J = 7.9 Hz, 2CH<sub>carbaz</sub>), 8.81 (1H, d, <sup>3</sup>J = 7.9 Hz, CH<sub>quinaz</sub>); <sup>19</sup>F NMR (CDCl<sub>3</sub>, 376 MHz) δ –61.29 (3F, s, CF<sub>3</sub>); EIMS *m/z* 633 [M + 2]<sup>+</sup> (10), 632 [M + 1]<sup>+</sup> (45), 631 [M]<sup>+</sup> (100), 344 (16), 342 (11), 315 (34), 264 (12), 241 (19), 230 (24), 201 (11); anal. C 76.06, H 3.83, N 11.09%, calcd for C<sub>40</sub>H<sub>24</sub>F<sub>3</sub>N<sub>5</sub> (631.66) C 76.04, H 3.80, N 11.15%.

#### 4. Conclusions

Nine push-pull molecules based on [1,2,4]triazolo[4,3-c]quinazolines were designed and synthesized by cross-coupling reactions. The structure of target compounds, namely the arrangement of the triazole ring, has been confirmed by means of the X-ray data method. The triazoloquinazolines **2** were shown to emit in solution and solid state. Photophysical properties (absorption, emission and QY) are influenced by the nature of arylamino residue, 3-aryltriazole fragment, as well as solvent polarity. Variations of structure and media can be used for the fine-tuning of characteristics that are necessary for practical application. Moreover, fluorophores display solvatochromic behavior and their emission maxima show bathochromic shifts with an increase in solvent polarity. Furthermore, changes in absorption and emission spectra upon the addition of water to MeCN solution, attributed to the aggregation process, have been shown. The twisted structure of fluorophores revealed by X-ray analysis can inhibit intermolecular π-π stacking interactions, thus favoring the strong solid-state emission and active aggregate forms. Additionally, triazoloquinazolines display reversible changes in color and optical properties upon the treatment with TFA and have the potential application as sensors. In general, this type of fluorophore represents a promising group of compounds for different applications and further investigation.

**Supplementary Materials:** The following supporting information can be downloaded at: <https://www.mdpi.com/article/10.3390/molecules28041937/s1>, Figures S1–S9: NMR and mass spectra of 3-aryl-5-aminobiphenyl substituted [1,2,4]triazolo[4,3-c]quinazolines **2a–i**; Tables S1–S4: Selected bond lengths and angles of compounds **2a**, **2e**; Figure S10: Planarity of compounds **2a** and **2e**; Figures S11–S23: Absorption and emission spectra of fluorophores **2a–i** in toluene and MeCN; Figure S24: Emission spectra of fluorophores **2a–i** in solid state; Tables S5–S8: Orientation polarizability for solvents (Δf), absorption and emission maxima (λ<sub>abs</sub>, λ<sub>em</sub>, nm) and Stokes shift (nm, cm<sup>−1</sup>) of compounds **2a**, **d**, **g**, **h** in different solvents; Figure S25: Fluorescence spectra of compound **2d** (a), **2g** (b), **2h** (c) in different solvents; Figures S26–S28: Absorption and emission behavior of compounds **2b**, **e**, **h** in MeCN/water mixture; Table S9, Figures S29–S31: Detailed data of the fluorescence lifetime measurements of **2b**, **2e**, **2h**. Figures S32 and S33: Absorption and fluorescence behavior of compounds **2e** and **2h** in acidic media.

**Author Contributions:** Conceptualization, V.N.C.; methodology, A.E.K.; investigation, A.E.K., E.S.S., G.A.K., V.S.G. and P.A.S.; writing—original draft preparation, T.N.M., E.V.N. and D.S.K.; writing—review and editing, G.N.L.; supervision, G.N.L. and E.V.N.; project administration, E.V.N. All authors have read and agreed to the published version of the manuscript.

**Funding:** The research funding from the Ministry of Science and Higher Education of the Russian Federation (Ural Federal University Program of Development within the Priority-2030 Program) is gratefully acknowledged.

**Institutional Review Board Statement:** Not applicable.

**Informed Consent Statement:** Not applicable.

**Data Availability Statement:** The data are available on request from the corresponding authors.

**Acknowledgments:** Our work was performed using «Uran» supercomputer of IMM UB RAS.

**Conflicts of Interest:** The authors declare no conflict of interest.

**Sample Availability:** Samples of compounds 2a–i are available from the authors.

## References

1. Singh, P.K.; Choudhary, S.; Kashyap, A.; Verma, H.; Kapil, S.; Kumar, M.; Arora, M.; Silakari, O. An Exhaustive Compilation on Chemistry of Triazolopyrimidine: A Journey through Decades. *Bioorg. Chem.* **2019**, *88*, 102919. [[CrossRef](#)] [[PubMed](#)]
2. Zuniga, E.S.; Korkegian, A.; Mullen, S.; Hembre, E.J.; Ornstein, P.L.; Cortez, G.; Biswas, K.; Kumar, N.; Cramer, J.; Masquelin, T.; et al. The Synthesis and Evaluation of Triazolopyrimidines as Anti-Tubercular Agents. *Bioorg. Med. Chem.* **2017**, *25*, 3922–3946. [[CrossRef](#)] [[PubMed](#)]
3. Jacobson, K.A.; Boeynaems, J.-M. P2Y Nucleotide Receptors: Promise of Therapeutic Applications. *Drug Discov. Today* **2010**, *15*, 570–578. [[CrossRef](#)] [[PubMed](#)]
4. Zhang, N.; Ayrál-Kaloustian, S.; Nguyen, T.; Hernandez, R.; Lucas, J.; Discafani, C.; Beyer, C. Synthesis and SAR of 6-Chloro-4-Fluoroalkylamino-2-Heteroaryl-5-(Substituted)Phenylpyrimidines as Anti-Cancer Agents. *Bioorg. Med. Chem.* **2009**, *17*, 111–118. [[CrossRef](#)] [[PubMed](#)]
5. El-Adl, K.; Ibrahim, M.-K.; Alesawy, M.S.I.; Eissa, I.H. [1,2,4]Triazolo[4,3-c]Quinazoline and Bis([1,2,4]Triazolo[4,3-*a'*,3'-c]Quinazoline Derived DNA Intercalators: Design, Synthesis, in Silico ADMET Profile, Molecular Docking and Anti-Proliferative Evaluation Studies. *Bioorg. Med. Chem.* **2021**, *30*, 115958. [[CrossRef](#)]
6. El-Adl, K.; Ibrahim, M.; Alesawy, M.S.; Eissa, I.H. Triazoloquinazoline Derived Classical DNA Intercalators: Design, Synthesis, in Silico ADME Profile, Docking, and Antiproliferative Evaluations. *Arch. Pharm.* **2022**, *355*, 2100506. [[CrossRef](#)]
7. Burbiel, J.C.; Ghattas, W.; Küppers, P.; Köse, M.; Lacher, S.; Herzner, A.-M.; Kombu, R.S.; Akkinpally, R.R.; Hockemeyer, J.; Müller, C.E. 2-Amino[1,2,4]Triazolo[1,5-c]Quinazolines and Derived Novel Heterocycles: Syntheses and Structure-Activity Relationships of Potent Adenosine Receptor Antagonists. *ChemMedChem* **2016**, *11*, 2272–2286. [[CrossRef](#)]
8. Zheng, Y.; Bian, M.; Deng, X.-Q.; Wang, S.-B.; Quan, Z.-S. Synthesis and Anticonvulsant Activity Evaluation of 5-Phenyl-[1,2,4]Triazolo[4,3-c]Quinazolin-3-Amines. *Arch. Pharm.* **2013**, *346*, 119–126. [[CrossRef](#)]
9. Esteban-Parra, G.M.; Sebastián, E.S.; Cepeda, J.; Sánchez-González, C.; Rivas-García, L.; Llopis, J.; Aranda, P.; Sánchez-Moreno, M.; Quirós, M.; Rodríguez-Diéguez, A. Anti-Diabetic and Anti-Parasitic Properties of a Family of Luminescent Zinc Coordination Compounds Based on the 7-Amino-5-Methyl-1,2,4-Triazolo[1,5-*a*]Pyrimidine Ligand. *J. Inorg. Biochem.* **2020**, *212*, 111235. [[CrossRef](#)]
10. Oukoloff, K.; Kovalevich, J.; Cornec, A.S.; Yao, Y.; Owyang, Z.A.; James, M.; Trojanowski, J.Q.; Lee, V.M.Y.; Smith, A.B.; Brunden, K.R.; et al. Design, Synthesis and Evaluation of Photoactivatable Derivatives of Microtubule (MT)-Active [1,2,4]Triazolo[1,5-*a*]Pyrimidines. *Bioorg. Med. Chem. Lett.* **2018**, *28*, 2180–2183. [[CrossRef](#)]
11. Eltyshv, A.K.; Agafonova, I.A.; Minin, A.S.; Pozdina, V.A.; Shevirin, V.A.; Slepukhin, P.A.; Benassi, E.; Belskaya, N.P. Photophysics, Photochemistry and Bioimaging Application of 8-Azapurine Derivatives. *Org. Biomol. Chem.* **2021**, *19*, 9880–9896. [[CrossRef](#)]
12. Taniya, O.S.; Fedotov, V.V.; Novikov, A.S.; Sadieva, L.K.; Krinochkin, A.P.; Kovalev, I.S.; Kopchuk, D.S.; Zyryanov, G.V.; Liu, Y.; Ulomsky, E.N.; et al. Abnormal Push-Pull Benzo[4,5]Imidazo[1,2-*a*][1,2,3]Triazolo[4,5-*e*]Pyrimidine Fluorophores in Planarized Intramolecular Charge Transfer (PLICT) State: Synthesis, Photophysical Studies and Theoretical Calculations. *Dyes Pigments* **2022**, *204*, 110405. [[CrossRef](#)]
13. Verbitskiy, E.V.; Gorbunov, E.B.; Baranova, A.A.; Lugovik, K.I.; Khokhlov, K.O.; Cheprakova, E.M.; Kim, G.A.; Rusinov, G.L.; Chupakhin, O.N.; Charushin, V.N. New 2*H*-[1,2,3]Triazolo[4,5-*e*][1,2,4]Triazolo[1,5-*a*]Pyrimidine Derivatives as Luminescent Fluorophores for Detection of Nitroaromatic Explosives. *Tetrahedron* **2016**, *72*, 4954–4961. [[CrossRef](#)]
14. Achelle, S.; Rodríguez-López, J.; Guen, F.R. Photoluminescence Properties of Aryl-, Arylvinyl-, and Arylethynylpyrimidine Derivatives. *ChemistrySelect* **2018**, *3*, 1852–1886. [[CrossRef](#)]
15. Sun, E.; Fang, R.; Liu, S.; Wu, J. Compound and Application Thereof. Patent CN113527302A, 22 October 2021.
16. Sun, E.; Fang, R.; Liu, S. Organic Compound for Light-Emitting Device, Application of Organic Compound and Organic Light-Emitting Device. Patent CN112174968A, 5 January 2021.
17. Sun, E.; Liu, S.; Feng, J.; Wu, J. Organic Electroluminescent Material and Organic Electroluminescent Device. Patent CN110256439A, 20 September 2019.
18. Moshkina, T.N.; Le Poul, P.; Barsella, A.; Pytela, O.; Bureš, F.; Robin-Le Guen, F.; Achelle, S.; Nosova, E.V.; Lipunova, G.N.; Charushin, V.N. Electron-Withdrawing Substituted Quinazoline Push-Pull Chromophores: Synthesis, Electrochemical, Photophysical and Second-Order Nonlinear Optical Properties. *Eur. J. Org. Chem.* **2020**, *2020*, 5445–5454. [[CrossRef](#)]
19. Moshkina, T.N.; Nosova, E.V.; Permyakova, J.V.; Lipunova, G.N.; Zhilina, E.F.; Kim, G.A.; Slepukhin, P.A.; Charushin, V.N. Push-Pull Structures Based on 2-Aryl/Thienyl Substituted Quinazolin-4(3*H*)-Ones and 4-Cyanoquinazolines. *Molecules* **2022**, *27*, 7156. [[CrossRef](#)]
20. Moshkina, T.N.; Nosova, E.V.; Permyakova, J.V.; Lipunova, G.N.; Valova, M.S.; Slepukhin, P.A.; Sadieva, L.K.; Charushin, V.N. Synthesis and Photophysical Properties of 2-Aryl-4-(Morpholin-4-yl)Quinazoline Chromophores: The Effect of  $\pi$ -Linker Moiety. *Dyes Pigments* **2022**, *206*, 110592. [[CrossRef](#)]
21. Nosova, E.V.; Kopotilova, A.E.; Ivan'kina, M.A.; Moshkina, T.N.; Kopchuk, D.S. Synthesis of 5-(4-Bromophenyl)- and 5-(5-Bromothiophen-2-yl)-Substituted 3-Aryl[1,2,4]Triazolo[4,3-*c*]Quinazolines. *Russ. Chem. Bull.* **2022**, *71*, 1483–1487. [[CrossRef](#)]

22. Mei, J.; Leung, N.L.C.; Kwok, R.T.K.; Lam, J.W.Y.; Tang, B.Z. Aggregation-Induced Emission: Together We Shine, United We Soar! *Chem. Rev.* **2015**, *115*, 11718–11940. [[CrossRef](#)]
23. Du, C.; Cheng, Z.; Shang, A.; Xu, Y.; Zhao, A.; Lei, C.; Chang, Y.; Lv, Y.; Lu, P. Two Different Implementation Strategies for Highly Efficient Non-Doped Fluorescent Organic Light-Emitting Diodes Based on Benzothiadiazole Derivatives. *Chem. Eng. J.* **2022**, *435*, 135010. [[CrossRef](#)]
24. Suman, G.R.; Pandey, M.; Chakravarthy, A.S.J. Review on New Horizons of Aggregation Induced Emission: From Design to Development. *Mater. Chem. Front.* **2021**, *5*, 1541–1584. [[CrossRef](#)]
25. Wan, Q.; Zhang, B.; Tong, J.; Li, Y.; Wu, H.; Zhang, H.; Wang, Z.; Pan, Y.; Tang, B.Z. Feasible Structure-Modification Strategy for Inhibiting Aggregation-Caused Quenching Effect and Constructing Exciton Conversion Channels in Acridone-Based Emitters. *Phys. Chem. Chem. Phys.* **2019**, *21*, 9837–9844. [[CrossRef](#)] [[PubMed](#)]
26. Xu, W.; Lee, M.M.S.; Zhang, Z.; Sung, H.H.Y.; Williams, I.D.; Kwok, R.T.K.; Lam, J.W.Y.; Wang, D.; Tang, B.Z. Facile Synthesis of AIEgens with Wide Color Tunability for Cellular Imaging and Therapy. *Chem. Sci.* **2019**, *10*, 3494–3501. [[CrossRef](#)] [[PubMed](#)]
27. Lakowicz, J.R. *Principles of Fluorescence Spectroscopy*, 3rd ed.; Lakowicz, J.R., Ed.; Springer: Boston, MA, USA, 2006; ISBN 978-0-38731-278-1.
28. Lippert, E. Spektroskopische Bestimmung Des Dipolmomentes Aromatischer Verbindungen Im Ersten Angeregten Singulettzustand. *Z. Für Elektrochem. Ber. Der Bunsenges. Für Phys. Chemie* **1957**, *61*, 962–975. [[CrossRef](#)]
29. Mataga, N.; Kaifu, Y.; Koizumi, M. Solvent Effects upon Fluorescence Spectra and the Dipolemoments of Excited Molecules. *Bull. Chem. Soc. Jpn.* **1956**, *29*, 465–470. [[CrossRef](#)]
30. Mukhopadhyay, A.; Maka, V.K.; Moorthy, J.N. Remarkable Influence of ‘Phane Effect’ on the Excited-State Properties of Cofacially Oriented Coumarins. *Phys. Chem. Chem. Phys.* **2017**, *19*, 4758–4767. [[CrossRef](#)]
31. Kosower, E.M. *An Introduction to Physical Organic Chemistry*; Wiley: New York City, NY, USA, 1968.
32. Kosower, E.M. The Effect of Solvent on Spectra. I. A New Empirical Measure of Solvent Polarity: Z-Values. *J. Am. Chem. Soc.* **1958**, *80*, 3253–3260. [[CrossRef](#)]
33. Dimroth, K.; Reichardt, C.; Siepmann, T.; Bohlmann, F. Über Pyridinium-N-Phenol-Betaine Und Ihre Verwendung Zur Charakterisierung Der Polarität von Lösungsmitteln. *Justus Liebigs Ann. Chem.* **1963**, *661*, 1–37. [[CrossRef](#)]
34. Richard, P. 2-Aryl-4(3H)Quinazolinones. *J. Heterocycl. Chem.* **1971**, *8*, 699–702.
35. Moshkina, T.N.; Nosova, E.V.; Kopotilova, A.E.; Savchuk, M.I.; Nikonov, I.L.; Kopchuk, D.S.; Slepukhin, P.A.; Kim, G.A.; Lipunova, G.N.; Charushin, V.N. Synthesis and Photophysical Properties of Pyridyl- and Quinolonyl-Substituted 4-(4-Aminophenyl)Quinazolines. *J. Photochem. Photobiol. A Chem.* **2022**, *429*, 113917. [[CrossRef](#)]
36. Varghese, A.; Akshaya, K.B. Application of Fluorescence in Solvatochromic Studies of Organic Compounds. In *Reviews in Fluorescence 2017*; Geddes, C.D., Ed.; Springer International Publishing: New York, NY, USA, 2018; pp. 99–121.
37. Ilharco, L.M.; Brito de Barros, R. Aggregation of Pseudoisocyanine Iodide in Cellulose Acetate Films: Structural Characterization by FTIR. *Langmuir* **2000**, *16*, 9331–9337. [[CrossRef](#)]
38. Jia, W.B.; Wang, H.W.; Yang, L.M.; Lu, H.B.; Kong, L.; Tian, Y.P.; Tao, X.T.; Yang, J.X. Synthesis of Two Novel Indolo[3,2-*b*]Carbazole Derivatives with Aggregation-Enhanced Emission Property. *J. Mater. Chem. C* **2013**, *1*, 7092–7101. [[CrossRef](#)]
39. Das, P.; Kumar, A.; Chowdhury, A.; Mukherjee, P.S. Aggregation-Induced Emission and White Luminescence from a Combination of  $\pi$ -Conjugated Donor-Acceptor Organic Luminogens. *ACS Omega*. **2018**, *3*, 13757–13771. [[CrossRef](#)]
40. Valeur, B.; Berberan-Santos, M.N. *Molecular Fluorescence*; Wiley: Hoboken, NJ, USA, 2012; Volume 53, ISBN 978-3-52732-837-6.
41. Krishnan, R.; Binkley, J.S.; Seeger, R.; Pople, J.A. Self-Consistent Molecular Orbital Methods. XX. A Basis Set for Correlated Wave Functions. *J. Chem. Phys.* **1980**, *72*, 650–654. [[CrossRef](#)]
42. McLean, A.D.; Chandler, G.S. Contracted Gaussian Basis Sets for Molecular Calculations. I. Second Row Atoms, Z=11–18. *J. Chem. Phys.* **1980**, *72*, 5639–5648. [[CrossRef](#)]
43. Clark, T.; Chandrasekhar, J.; Spitznagel, G.W.; Schleyer, P.V.R. Efficient Diffuse Function-augmented Basis Sets for Anion Calculations. III. The 3-21+G Basis Set for First-row Elements, Li–F. *J. Comput. Chem.* **1983**, *4*, 294–301. [[CrossRef](#)]
44. Frisch, M.J.; Pople, J.A.; Binkley, J.S. Self-Consistent Molecular Orbital Methods 25. Supplementary Functions for Gaussian Basis Sets. *J. Chem. Phys.* **1984**, *80*, 3265–3269. [[CrossRef](#)]
45. Neese, F. The ORCA Program System. *Wiley Interdiscip. Rev. Comput. Mol. Sci.* **2012**, *2*, 73–78. [[CrossRef](#)]
46. Dolomanov, O.V.; Bourhis, L.J.; Gildea, R.J.; Howard, J.A.K.; Puschmann, H. OLEX2: A Complete Structure Solution, Refinement and Analysis Program. *J. Appl. Crystallogr.* **2009**, *42*, 339–341. [[CrossRef](#)]
47. Sheldrick, G.M. A Short History of SHELX. *Acta Crystallogr. Sect. A Found. Crystallogr.* **2008**, *64*, 112–122. [[CrossRef](#)]

**Disclaimer/Publisher’s Note:** The statements, opinions and data contained in all publications are solely those of the individual author(s) and contributor(s) and not of MDPI and/or the editor(s). MDPI and/or the editor(s) disclaim responsibility for any injury to people or property resulting from any ideas, methods, instructions or products referred to in the content.